

Visible quantum cutting through downconversion in green-emitting $\text{K}_2\text{GdF}_5 : \text{Tb}^{3+}$ phosphors

Te-Ju Lee, Li-Yang Luo, Eric Wei-Guang Diau, Teng-Ming Chen, Bing-Ming Cheng, and Chien-Yueh Tung

Citation: *Applied Physics Letters* **89**, 131121 (2006); doi: 10.1063/1.2358193

View online: <http://dx.doi.org/10.1063/1.2358193>

View Table of Contents: <http://scitation.aip.org/content/aip/journal/apl/89/13?ver=pdfcov>

Published by the [AIP Publishing](#)

Articles you may be interested in

Enhanced near-infrared quantum cutting in $\text{GdBO}_3 : \text{Tb}^{3+}$, Yb^{3+} phosphors by Ce^{3+} codoping

J. Appl. Phys. **106**, 113521 (2009); 10.1063/1.3267484

Vacuum ultraviolet spectroscopic properties of rare earth ($\text{RE} = \text{Ce}$, Tb , Eu , Tm , Sm) -doped hexagonal $\text{KCaGd}(\text{PO}_4)_2$ phosphate

J. Appl. Phys. **102**, 093514 (2007); 10.1063/1.2800172

Cooperative downconversion in $\text{GdAl}_3(\text{BO}_3)_4 : \text{RE}^{3+}$, Yb^{3+} ($\text{RE} = \text{Pr}$, Tb , and Tm)

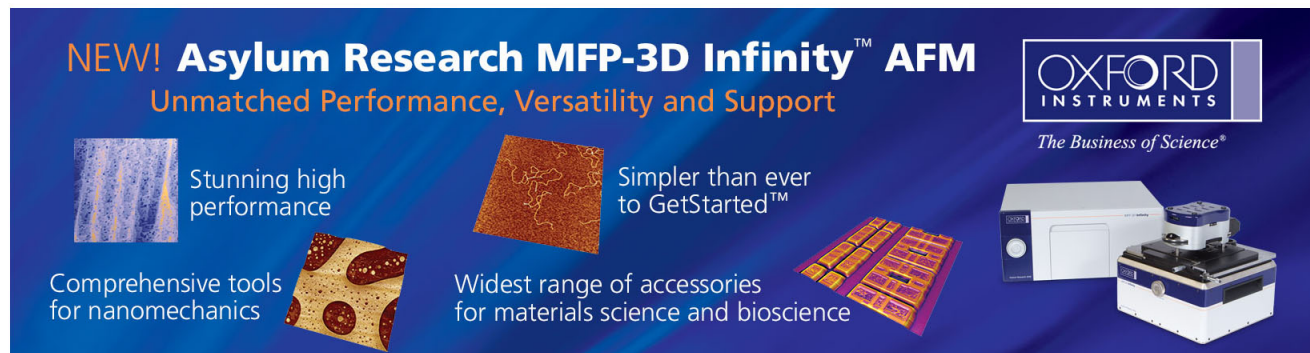
Appl. Phys. Lett. **91**, 051903 (2007); 10.1063/1.2757595

Concentration-dependent near-infrared quantum cutting in $\text{GdBO}_3 : \text{Tb}^{3+}$, Yb^{3+} nanophosphors

Appl. Phys. Lett. **90**, 061914 (2007); 10.1063/1.2472195

Visible quantum cutting through downconversion in $\text{KLiGdF}_5 : \text{Eu}^{3+}$ crystals


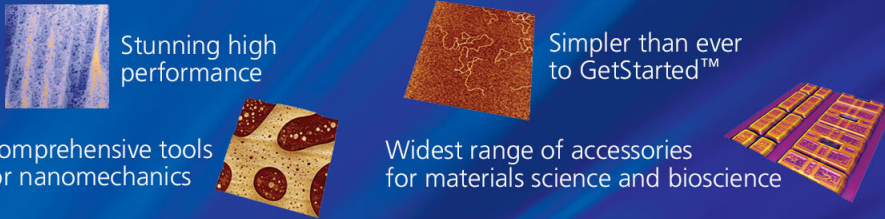
J. Appl. Phys. **98**, 103515 (2005); 10.1063/1.2135893



NEW! Asylum Research MFP-3D Infinity™ AFM
Unmatched Performance, Versatility and Support

OXFORD INSTRUMENTS
The Business of Science®

Stunning high performance
Simpler than ever to GetStarted™
Comprehensive tools for nanomechanics
Widest range of accessories for materials science and bioscience



Visible quantum cutting through downconversion in green-emitting $K_2GdF_5:Tb^{3+}$ phosphors

Te-Ju Lee, Li-Yang Luo, Eric Wei-Guang Diau, and Teng-Ming Chen^{a)}
Department of Applied Chemistry, National Chiao Tung University, Hsinchu 30010, Taiwan

Bing-Ming Cheng
National Synchrotron Radiation Research Center, Hsinchu 30076, Taiwan

Chien-Yueh Tung
Union Chemical Laboratories, Industrial Technology Research Institute, Hsinchu 30011, Taiwan

(Received 5 February 2006; accepted 6 September 2006; published online 29 September 2006)

Visible quantum cutting under excitations at 212 and 172 nm in a green-emitting phosphor $K_2GdF_5:Tb^{3+}$ (11%) via a downconversion mechanism is investigated. The authors measured the vacuum ultraviolet (VUV) excitation and emission spectra and proposed mechanisms to rationalize the quantum-cutting effect. One short-UV or one VUV photon absorbed by Tb^{3+} is split into multiple visible photons emitted by Tb^{3+} through cross relaxation and direct energy transfer. Calculations indicate an optimal quantum efficiency as great as 189% for this phosphor. © 2006 American Institute of Physics. [DOI: 10.1063/1.2358193]

As the energy of a vacuum ultraviolet (VUV) photon ($\lambda < 200$ nm) is more than twice that of a visible photon, there is enough energy for emission of two visible photons for each VUV photon absorbed, a phenomenon called quantum cutting (QC). Intensive research activity has focused on QC by rare-earth-doped phosphors in the VUV region,^{1–10} mainly because VUV-excited phosphors are indispensable for applications of plasma display panels and mercury-free lighting. Fluoride materials doped with trivalent rare-earth ions provide an excellent opportunity to develop materials suitable for applications with VUV radiation as an excitation source. In particular, the systems nMF_2-mGdF_3 [$M=Li$,^{3,8} Na,⁹ K,^{9,10} and Cs (Ref. 6)] were actively investigated as effective host matrices to realize QC phosphors, whereas systems xAF_2-yGdF_3 (A being a group-II element) were little investigated. The design of QC phosphors requires appropriate combinations of $R_1^{3+}-R_2^{3+}$ or $R_1^{3+}-R_2^{3+}-R_3^{3+}$ ($R_1=Gd$, $R_2=Eu$ and Tb , and $R_3=Er$) as activator ion-pairs or couples and relevant VUV spectral data. Quantum cutting via downconversion has been widely witnessed for many rare-earth-based phosphors;^{1–10} the greatest quantum efficiency (QE) in the visible spectral region was observed for $LiGdF_4:Eu$ (190%) (Ref. 3) and $BaF_2:Gd, Eu$ (194%) (Ref. 4) phosphors.

Motivated by the few reported QC phosphors containing solely Pr^{3+} (Refs. 1 and 2) or couples $Gd^{3+}-Eu^{3+}$,^{3,4} $Gd^{3+}-Er^{3+}$,⁵ and $Gd^{3+}-Tb^{3+}-Er^{3+}$ (Ref. 6) and seeking potential phosphors showing a QC effect, we have investigated $KF-GdF_3$ systems doped with rare-earth ions Eu^{3+} , Tb^{3+} , and Er^{3+} as activators. Here we report the QC phenomenon of a green-emitting phosphor $K_2(Gd_{1-x}Tb_x)F_5$ [$x=1\%$, 3%, 5%, 9%, and 11%, abbreviated $K_2GdF_5:Tb^{3+}$ ($x\%$)] that crystallizes in a structure of K_2LnF_5 type according to Güde and Hebecker;¹¹ therein Gd^{3+} (or Ln^{3+}) is coordinated with seven fluoride anions. Our results show that the optimal quantum efficiencies (η) of $K_2GdF_5:Tb^{3+}$ in the visible re-

gion are 189% and 187% under excitations at 212 and 172 nm, respectively.

Polycrystalline samples of $K_2GdF_5:Tb^{3+}$ ($x\%$) ($x=1\%$, 3%, 5%, 9%, and 11%) doped with specified levels of Tb^{3+} were synthesized on firing stoichiometric reactants at 600 °C for 8 h in a sealed tube. The phase purity of all $K_2GdF_5:Tb^{3+}$ samples was verified using powder x-ray diffraction (XRD) analysis (Bruker AXS D8 advanced automatic diffractometer). For spectral measurements of steady-state emission and excitation with a synchrotron source, the intense and continuous VUV beam was dispersed from a beam line with a cylindrical grating monochromator coupled to the 1.5 GeV storage ring at the National Synchrotron Radiation Research Center in Taiwan; this beam line has four gratings and a focal length of 6 m. We used a grating (450 grooves/mm) that spans the wavelength range of 100–350 nm. The emission from the phosphor was analyzed with a monochromator (0.32 m) and detected with a photomultiplier in a photon-counting mode. Time-resolved measurements were performed with a tunable nanosecond optical-parametric-oscillator/Q-switch-pumped neodymium doped yttrium aluminum garnet laser system (NT341/1/UV, Ekspla). Emission transients were collected with a monochromator (SpectraPro-300i, ARC), detected with a photomultiplier tube (R928HA, Hamamatsu) connected to a digital oscilloscope (LT372, LeCroy), and transferred to a computer for kinetic analysis.¹²

The experimental XRD profile for $K_2GdF_5:Tb^{3+}$ (5%) agrees satisfactorily with that calculated with the software CRYSTALLOGRAPHICA (Ref. 13) (supporting data in Fig. A); both are consistent with that reported by Güde and Hebecker.¹¹ Shown in Fig. 1 is the VUV excitation spectrum for $K_2GdF_5:Tb^{3+}$ (5%) monitored at 542 and 415 nm, respectively; the strong, broad excitation lines centered at 212 and 172 nm are assigned as spin-allowed transitions from state 7F_6 to low-spin (LS) states $4f^75d$ of Tb^{3+} .^{4,14} The broad absorption of Tb^{3+} at 212 nm in the excitation spectrum also supports the origin of absorption being attributed to a transition $4f \rightarrow 4f5d$ (LS).^{4,14} The much weaker emission line at

^{a)}Electronic mail: tmchen@mail.nctu.edu.tw

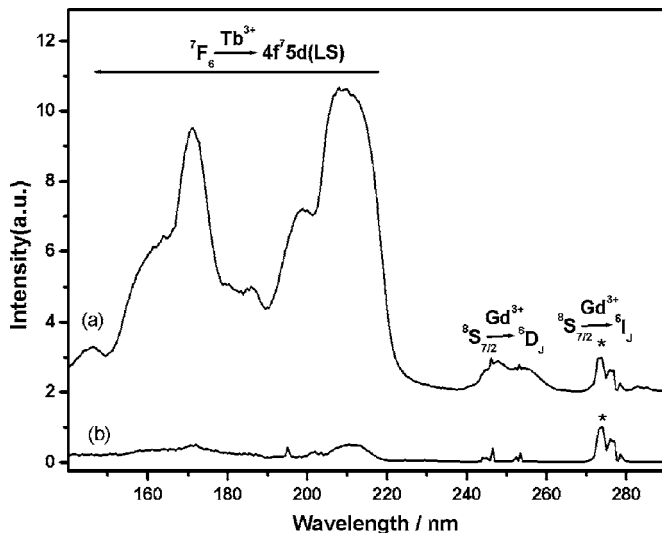


FIG. 1. Excitation spectra of $\text{K}_2\text{GdF}_5:\text{Tb}^{3+}$ (5%) monitored at (a) $\lambda_{\text{em}} = 542 \text{ nm}$ (${}^5\text{D}_4 \rightarrow {}^7\text{F}_5$ of Tb^{3+}) and (b) $\lambda_{\text{em}} = 415 \text{ nm}$ (${}^5\text{D}_3 \rightarrow {}^7\text{F}_5$ of Tb^{3+}). The spectra are scaled to the ${}^8\text{S}_{7/2} \rightarrow {}^6\text{I}_J$ excitation intensity (*).

274 nm is assigned as excitations from the ground state ${}^8\text{S}_{7/2}$ to state ${}^6\text{I}_J$ of Gd^{3+} .

Using the emission feature attributed to transition ${}^5\text{D}_3 \rightarrow {}^7\text{F}_5$ as a reference, we normalized the emission spectra, shown in Figs. 2(a)–2(c), of $\text{K}_2\text{GdF}_5:\text{Tb}^{3+}$ (5%) under three excitation conditions of 274, 212, and 172 nm, respectively. To rationalize the observations of visible QC and energy transfer revealed in Figs. 2(b) and 2(c), we depict in Fig. 3 simplified diagrams of energy of $\text{K}_2\text{GdF}_5:\text{Tb}^{3+}$ that explain visible QC with a two-step energy transfer. Several possible pathways involved in the QC downconversion include excitation, relaxation, energy transfer, and nonradiative relaxation, depending on the excitation wavelength.

As Fig. 2(a) indicates, beyond the emission at 315 nm that is attributed to ${}^6\text{P}_{7/2} \rightarrow {}^8\text{S}_{7/2}$ of Gd^{3+} , we observed multiple emissions appearing in spectral region of 350–650 nm that we attribute to transitions from levels ${}^5\text{D}_3$ and ${}^5\text{D}_4$ of Tb^{3+} , respectively, when $\text{K}_2\text{GdF}_5:\text{Tb}^{3+}$ is excited at 274 nm. This observation is further rationalized through Gd^{3+} being

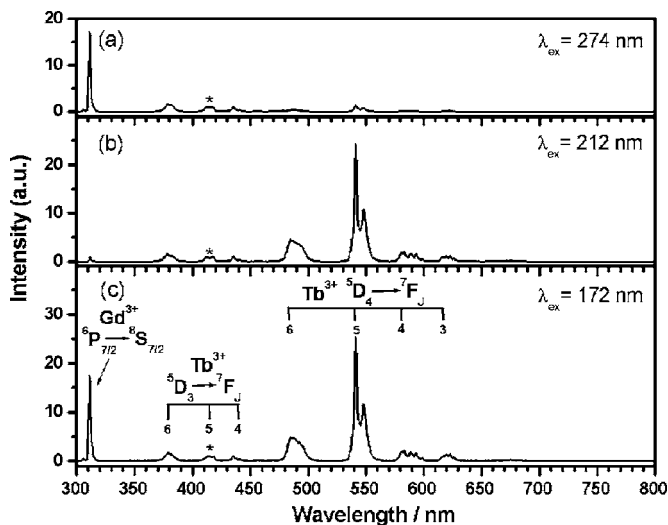


FIG. 2. Emission spectra of $\text{K}_2\text{GdF}_5:\text{Tb}^{3+}$ (5%) excited at $\lambda_{\text{ex}} =$ (a) 274, (b) 212, and (c) 172 nm. The spectra are scaled to the ${}^5\text{D}_3 \rightarrow {}^7\text{F}_5$ excitation intensity (*).

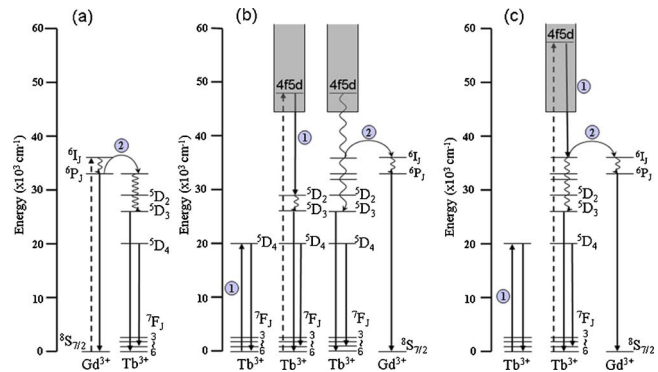


FIG. 3. (Color online) Schematic energy levels of $\text{K}_2\text{GdF}_5:\text{Tb}^{3+}$ showing possible mechanisms for visible QC under excitation of VUV with $\lambda_{\text{ex}} =$ (a) 274, (b) 212, and (c) 172 nm; ① and ② denote cross relaxation and direct energy transfer, respectively.

excited to level ${}^6\text{I}_J$ and relaxing readily to state ${}^6\text{P}_{7/2}$ nonradiatively when direct energy transfer from ${}^6\text{P}_{7/2}$ to the neighboring Tb^{3+} ion or radiative relaxation of Gd^{3+} from ${}^6\text{P}_{7/2}$ to ${}^8\text{S}_{7/2}$ occurs [cf. Fig. 3(a)]. The intensity of emissions from level ${}^5\text{D}_3$ of Tb^{3+} is comparable with those observed on excitations at 212 and 172 nm, whereas that from level ${}^5\text{D}_4$ under excitation at 274 nm is much weaker. These observations are consistent with the diagram of energy levels in Fig. 3(a). We conclude that no visible QC occurs when UV radiation at 274 nm serves to excite $\text{K}_2\text{GdF}_5:\text{Tb}^{3+}$.

As indicated in Figs. 2(b) and 3(b), when $\text{K}_2\text{GdF}_5:\text{Tb}^{3+}$ (5%) is excited at 212 nm, Tb^{3+} becomes pumped to level $4f^7 5d$, and subsequently relaxes from that high-lying energy level to an intermediate state ${}^5\text{D}_2$; the released energy is transferred to a neighboring Tb^{3+} by cross relaxation (step 1), which then serves to excite Tb^{3+} to level ${}^5\text{D}_4$ resulting in the observed green luminescence. In addition, in the relaxation that takes Tb^{3+} from state $4f^7 5d$ to levels ${}^5\text{D}_3$ and ${}^5\text{D}_4$, the released energy is transferred directly to the neighboring Gd^{3+} (step 2), which is responsible for UV luminescence of Gd^{3+} observed at 315 nm [cf. Figs. 2(b) and 2(c)]. The photoluminescence (PL) intensity of $\text{Tb}^{3+} {}^5\text{D}_4 \rightarrow {}^7\text{F}_J$ transitions dominates over that of ${}^5\text{D}_3 \rightarrow {}^7\text{F}_J$, which we attribute to a much greater probability of transitions of the former, as indicated in Figs. 3(b) and 3(c). As revealed in Fig. 2(c), with excitation at 172 nm, similar but much stronger [relative to Fig. 2(a)] emission of $\text{K}_2\text{GdF}_5:\text{Tb}^{3+}$ (5%) was observed. The mechanism to rationalize the observed visible QC in Fig. 2(c) includes excitation, cross relaxation, and direct energy transfer, similar to our discussion of that observed in $\text{K}_2\text{GdF}_5:\text{Tb}^{3+}$ (5%) excited at 212 nm.

For measurements of time-resolved emission, we used two laser excitation wavelengths— $\lambda_{\text{ex}} = 274$ and 215 nm—to pump Gd^{3+} and Tb^{3+} , respectively; the corresponding decays appear in Fig. 4. With excitation at $\lambda_{\text{ex}} = 274$ nm, the emission decays [Figs. 4(a) and 4(b)] feature three components; a dominant rapid component decays on a nanosecond scale (see supporting information) and two slow components fitted with a consecutive kinetic model, $A \rightarrow B \rightarrow C$; $\tau_1 = 0.7 \text{ ms}$ and $\tau_2 = 3.9$ and 7.2 ms at $\lambda_{\text{em}} = 415 \text{ nm}$ [Fig. 4(a)] and 542 nm [Fig. 4(b)], respectively. With excitation at $\lambda_{\text{ex}} = 215 \text{ nm}$, the transient behavior differs—the rapid component is negligible, as observed at $\lambda_{\text{em}} = 415 \text{ nm}$ [Fig. 4(c)] and 542 nm [Fig. 4(d)]. Furthermore, the slow component becomes a dominant part of the transient observed at $\lambda_{\text{em}} = 542 \text{ nm}$, con-

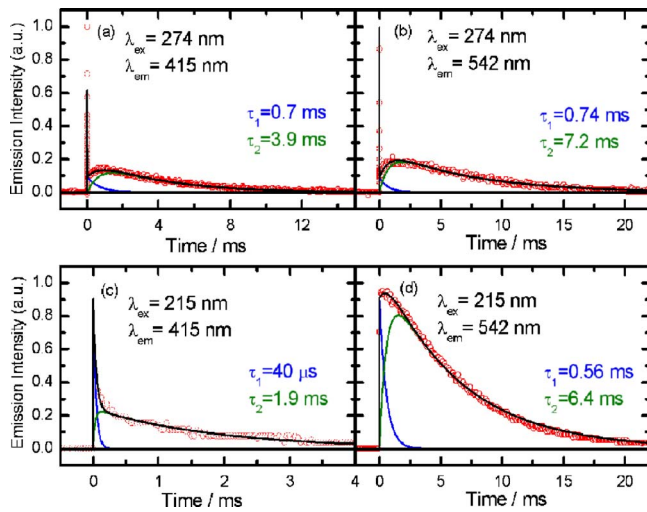


FIG. 4. (Color online) Emissive decays of $\text{K}_2\text{GdF}_5:\text{Tb}^{3+}$ (5%) at (a) $\lambda_{\text{ex}} = 274$ nm and $\lambda_{\text{em}} = 415$ nm, (b) $\lambda_{\text{ex}} = 274$ nm and $\lambda_{\text{em}} = 542$ nm, (c) $\lambda_{\text{ex}} = 215$ nm and $\lambda_{\text{em}} = 415$ nm, and (d) $\lambda_{\text{ex}} = 215$ nm and $\lambda_{\text{em}} = 542$ nm. The transients were fitted according to a consecutive kinetic model. The black solid curves are theoretical fits; blue and olive curves under each transient are deconvoluted components corresponding to A and B, respectively.

sistent with a cross-relaxation mechanism (step ①) shown in Fig. 3(b). Control experiments (cf. supporting data in Fig. B) indicate that energy relaxation in a pure K_2GdF_5 phosphor occurs on nanosecond and microsecond scales, supporting that the millisecond components shown in transients of Fig. 4 are due to direct energy transfer (step ②) and cross relaxation (step ①) with excitations at 274 and 215 nm, respectively.

For a practical calculation of extra quantum efficiency (η), some essential premises are proposed: the VUV absorption of phosphors should not be taken into account, and possible nonradiative losses due to energy migration at defects and impurities in samples must be ignored. For overall calculations of η involved in the QC processes, in addition to η_{DT} (i.e., 100%), we have calculated an extra η corresponding to cross relaxation (η_{CR}) from Tb^{3+} to a neighboring Tb^{3+} through QC with this equation proposed by Wegh *et al.*,^{3,4} later modified by Tzeng *et al.*¹⁵

$$\frac{P_{\text{CR}}}{P_{\text{CR}} + P_{\text{DT}}} = \frac{R(^5D_4/\text{rest})_{\text{Tb}^{3+}} - R(^5D_4/\text{rest})_{\text{Gd}^{3+}}}{R(^5D_4/\text{rest})_{\text{Tb}^{3+}} + 1}.$$

Here P_{CR} represents the probability for cross relaxation and P_{DT} is the probability for direct energy transfer. $R(^5D_4/\text{rest})$ is the ratio of PL intensity of 5D_4 to that attributed to 5D_3 of Tb^{3+} and $^6P_{7/2}$ of Gd^{3+} ; the subscript indicates excitation from Tb^{3+} or Gd^{3+} . With η_{DT} of a phosphor assumed to be 100%, the extra η for energy transfer via cross relaxation is 89% and 87% for excitations at 212 and 172 nm, respectively. Under these two excitations, that at 172 nm does not yield a greater QE, perhaps indicating a significant fraction of excitation energy being lost nonradiatively during QC, thus resulting in a decreased η for $\text{K}_2\text{GdF}_5:\text{Tb}^{3+}$.

TABLE I. η_{CR} calculated for $\text{K}_2\text{GdF}_5:\text{Tb}^{3+}$ ($x\%$) as a function of x for excitations at 212 and 172 nm.

x	η_{CR} (%)	
	λ_{ex} (nm)=212	λ_{ex} (nm)=172
1	75.0	70.3
3	80.6	79.3
5	84.9	83.7
9	86.7	86.0
11	89.1	87.3

We investigated also the dependence of the calculated η_{CR} on the concentration of Tb^{3+} doped into $\text{K}_2\text{GdF}_5:\text{Tb}^{3+}(x\%)$ under VUV excitations at 172 and 212 nm; the results are summarized in Table I. The general trend indicates that the calculated η_{CR} for $\text{K}_2\text{GdF}_5:\text{Tb}^{3+}(x\%)$ phosphors increases monotonically from 70% for a sample with $x=1\%$ to 87% for sample with $x=11\%$ under excitation at 172 nm. In contrast, the calculated η_{CR} for $\text{K}_2\text{GdF}_5:\text{Tb}^{3+}(x\%)$ phosphors increases from 75% for a sample with $x=1\%$ to 89% for a sample with $x=11\%$ under excitation at 212 nm.

In summary, we have discovered a green-emitting QC phosphor $\text{K}_2\text{GdF}_5:\text{Tb}^{3+}$ for which the visible quantum efficiency achieves 189% and 187% for VUV excitations at 212 and 172 nm, respectively. Upon excitation of Tb^{3+} with an energetic photon, two photons in the visible range are generated through a two-step process—cross relaxation and direct energy transfer—from one Tb^{3+} to a neighboring Tb^{3+} or Gd^{3+} with a quantum efficiency that exceeds 100%; for UV excitation at 274 nm no such QC effect was observed.

National Science Council of Taiwan supported this project under Contract No. NSC94-2113-M-009-001. National Synchrotron Radiation Research Center provided research facilities and resources.

¹W. W. Piper and F. S. Ham, *J. Lumin.* **8**, 344 (1974).

²J. L. Sommerdijk, A. Bril, and A. W. de Jager, *J. Lumin.* **8**, 341 (1974).

³R. T. Wegh, H. Donker, K. D. Oskam, and A. Meijerink, *Science* **283**, 663 (1999).

⁴R. T. Wegh, E. V. D. van Loef, and A. Meijerink, *J. Lumin.* **90**, 111 (2000).

⁵B. Liu, Y. Chen, C. Shi, H. Tang, and Y. Tao, *J. Lumin.* **101**, 155 (2003).

⁶N. M. Khaidukov, S. K. Lam, D. Lo, V. N. Makhov, and N. V. Suetin, *Opt. Mater. (Amsterdam, Neth.)* **19**, 365 (2002).

⁷K. D. Oskam, R. T. Wegh, H. Donker, E. V. D. van Loef, and A. Meijerink, *J. Alloys Compd.* **300/301**, 421 (2000).

⁸R. T. Wegh, H. Donker, and A. Meijerink, *Phys. Rev. B* **56**, 13841 (1997).

⁹F. You, S. Huang, S. Liu, and Y. Tao, *J. Lumin.* **110**, 95 (2004).

¹⁰N. Kodama and Y. Watanabe, *Appl. Phys. Lett.* **84**, 4141 (2004).

¹¹K. Güde and C. Hebecker, *Z. Naturforsch. B* **40**, 864 (1985).

¹²L. Y. Luo, C. F. Lo, C. Y. Lin, I. J. Chang, and Eric W. G. Diau, *J. Phys. Chem. B* **110**, 410 (2006).

¹³CRYSTALLOGRAPHICA, v. 1.50a, Oxford Cryosystems, Oxford, UK, 1995–1998.

¹⁴L. van Pieterse, M. F. Reid, G. W. Burdick, and A. Meijerink, *Phys. Rev. B* **65**, 045114 (2002).

¹⁵H. Y. Tzeng, B. M. Cheng, and T. M. Chen, *J. Lumin.* (in press).